Journal of Hazardous Materials 176 (2010) 146–153

Contents lists available at ScienceDirect

Journal of Hazardous Materials

journal homepage: www.elsevier.com/locate/jhazmat

Mathematical modeling of velocity and number density profiles of particles across the flame propagation through a micro-iron dust cloud

Mehdi Bidabadi*, Ali Haghiri, Alireza Rahbari

Department of Mechanical Engineering, Iran University of Science and Technology (IUST), Combustion Research Laboratory, Narmak, Hangam St., Tehran, Iran

ARTICLE INFO

Article history:
Received 2 August 2009
Received in revised form 25 October 2009
Accepted 31 October 2009
Available online 10 November 2009

Keywords:
Thermophoretic force
Analytical approach
Dust explosion hazard
Velocity profile
Concentration profile

ABSTRACT

In this study, an attempt has been made to analytically investigate the concentration and velocity profiles of particles across flame propagation through a micro-iron dust cloud. In the first step, Lagrangian particle equation of motion during upward flame propagation in a vertical duct is employed and then forces acting upon the particle, such as thermophoretic force (resulted from the temperature gradient), gravitation and buoyancy are introduced; and consequently, the velocity profile as a function of the distance from the leading edge of the combustion zone is extracted. In the resumption, a control volume above the leading edge of the combustion zone is considered and the change in the particle number density in this control volume is obtained via the balance of particle mass fluxes passing through it. This study explains that the particle concentration at the leading edge of the combustion zone is more than the particle agglomeration in a distance far from the flame front. This increase in the particle aggregation above the combustion zone has a remarkable effect on the lower flammability limits of combustible particle cloud. It is worth noticing that the velocity and particle concentration profiles show a reasonable compatibility with the experimental data.

1. Introduction

Dust explosion is one of the most challenging and dangerous hazards in industries that manufacture, process, generate, or use combustible dusts. It has been a recognized threat to humans and property for the last 150 years [1]; hence, an accurate knowledge of the explosion hazards is essential [2].

With the advancement of powder technology and the increase of powder handling processes, hazard assessment and the establishment of preventive methods for dust explosions have become more important from the view point of industrial loss prevention. In spite of significant efforts to obtain information on the explosibility of dusts, the fundamental mechanisms of flame propagation in dust suspension have not been studied sufficiently [3,4].

Associating with the importance of dust explosion and flame propagation through dust particles, Sun et al. [5–8] experimentally examined the behavior of iron particles near the combustion zone across upward and downward flame propagating and consequently, the velocity and number density profiles of particles were calculated from these researches. Similarly, the same study has been carried out by Han et al. [9]. They experimentally explained the flame propagation mechanism through lycopodium dust cloud based on dust particles' behavior. Cashdollar and Zlochower [10] conducted a study of the explosibility of various metals and other elemental dusts, with a focus on the experimental explosion temperatures.

Bidabadi and Rahbari [11] analytically investigated the flame propagation through lycopodium dust particles and explored the flame structure mechanism and the effect of temperature difference between gas and particles on the combustion characteristics. In another study, Bidabadi and Rahbari [12] presented a novel analytical model for predicting the heat loss and Lewis number effects on the combustion of lycopodium particles.

Furthermore, in our previous study [13], various aspects of flame propagation and the structure of combustion zone were analytically investigated and the effects of different Lewis and Damköhler numbers and the initiation of particles vaporization on the combustion phenomenon of the organic dust particles were completely specified.

One of the important phenomena in flame propagation through a combustible mixture of dust particles and air is the impact of temperature gradient (i.e., thermophoretic force) on dynamic behavior of particles which has found numerous applications in the aerosol technology field. In a temperature gradient field, small particles move in the direction opposite to the temperature gradient, resulting in the thermophoresis which has a significant influence on the behavior of soot particles. Thus, in explaining the transport of soot particles, the consideration of thermophoretic effect is essential,

* Corresponding author. Tel.: +98 21 77 240 197; fax: +98 21 77 240 488.
E-mail address: bidabadi@iust.ac.ir (M. Bidabadi).

0304-3894/$ – see front matter © 2009 Elsevier B.V. All rights reserved.
doi:10.1016/j.jhazmat.2009.10.130

as demonstrated by Gomez and Rosner [14] for diffusion flames. In addition, thermophoretic effects on spherical aerosol particles have been studied extensively for a wide range of temperatures and flow conditions [15–17]. Batchelor and Shen [18] investigated the thermophoretic deposition of particles flowing over a cold surface. There are several researches investigating the amount of soot deposition to solid media inserted in diffusion flames [19,20], demonstrating that sharp temperature gradient by the existence of cold solid surface induced the thermophoretic effect and promoted soot deposition. However, Ono et al. [21,22] reported that the thermophoretic velocities evaluated by the two equations are much smaller than the values measured in their experiments independent of agglomeration size. They also showed that soot agglomerates under thermophoretic forces behave as individual fine primary particles in the free-molecular regime rather than as large size particles in the slip-flow regime.

Tsai and Liang [23] presented a rational correlation for evaluating the effect of thermophoresis on aerosol particle deposition from laminar flow systems. Zheng [24] reviewed the existing theories and data in two major categories, for spherical particles and for non-spherical particles, as well as the various techniques in making thermophoresis measurements. Wang [25] explained the effect of thermophoresis on particle deposition rate from a natural convection flow. Walsh et al. [26] developed a model in order to investigate the thermophoretic deposition of aerosol particles on the wall of a relatively cool cylindrical tube.

A one-dimensional, steady-state theoretical analysis of flame propagation mechanism through micro-iron dust particles based on dust particles' behavior with special remark on the thermophoretic force for small Knudsen numbers (i.e., near continuum limit) is presented in this paper. A discrete trajectory approach (Lagrangian method) is proposed and the physical mechanisms controlling particle transport such as gravitation, buoyancy and thermophoretic forces are taken into account. Consequently, the number density and velocity profiles of particles near a flame propagating through an iron particle cloud are analytically determined. This study shows that the number density profile of micro-iron particles across the leading edge of the flame front decreases with increase in the distance from the combustion zone leading edge. It is worth noticing that the present analytical model is specifically suitable for further improvement of numerical computer codes (e.g., Dust Explosion Simulation Code (DESC)) to simulate the flame propagation in accidental dust explosions involving fine iron dust. In a broader perspective, this kind of simulation becomes more important in tailoring systems for dust explosion isolation, venting and suppression. Moreover, the measured profiles of velocity and number density of iron particles are in a good agreement with the published experimental results.

2. Lagrangian iron particle equation of motion

In the present study, it is assumed that the micro-iron particles are suspended in air and ignited by an electric spark near the bottom end of a vertical duct, and then flame propagates upwardly through combustible dust mixture in this duct, as seen in Fig. 1(a). It should be noted that there is a strict distinction between flame velocity and burning velocity. So that, the flame speed (flame velocity) is obtained from camcorder records by measuring the time interval for the flame to propagate a known distance between two markers, but a volumetric consumption rate of reactant per unit flame area is known as burning velocity. The reactive mixture expands quickly during the combustion phenomenon and hence, the flame seems to be a moving piston acting on both the burned and unburned mixtures, leading to an increase in gas density in

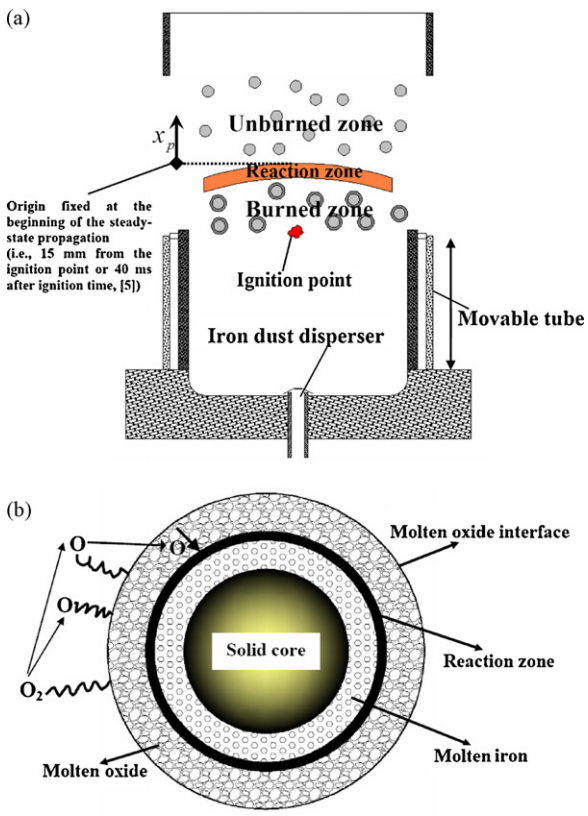

Fig. 1. (a) The flame structure of the combustible mixture of micro-iron dust particles and air; (b) the schematic of iron oxidation process at the combustion reaction.

front of the flame front and acting as an expansion flow in the flow field. Consequently, the iron dust particles follow the bulk gaseous motion in the unburned zone to form a distribution of particles concentration toward the leading edge of the combustion zone.

It is worth noticing that the turbulence within the chamber is induced by both the jetting effects of pneumatic dispersion systems and the shear layer near the chamber wall owing to the expansion of combustion products. The turbulence increases [27] the combustion reaction rate around the combustion zone and enhances the heat transport among the particles. This will lead to the acceleration of the flame propagation. But in the most experimental studies (e.g., Sun et al. [5,7,8]) carried out on the flame propagation through particle cloud, the main effort was to reduce the aforementioned factors. In order to decrease the jetting effects of pneumatic dispersion systems in inducing the turbulence in the combustion process, the following instructions are used by the researchers:

The dust is dispersed at the base of a conical chamber through the impact of a high velocity cylindrical jet issuing from an adjustable circular slot. A combustion chamber where combustion experiments are performed is connected to the dispersion chamber through an 8° conical diffuser. The diffuser provides expansion and laminarization of the dust flow which is initially turbulent in the dust disperser [28]. In addition, a set of quenching plates with a gap about 3.5 mm between plates is also installed in the beneath part of the chamber. This set serves as a flame arrestor to prevent flash back into the dispersion system and also helps to laminarize the dust flow after it exits from the dust disperser.

Furthermore, in order to annihilate the tube wall effect in inducing the turbulence generation during the flame propagation

through iron dust particles, a special method in the experimental setup was presented by Sun et al. [5,7,8]. In this experimental apparatus, the combustion chamber shown in Fig. 1(a) is provided with a movable tube. Before the movable tube starts to move down, the iron dust is dispersed by air into the combustion chamber. Just after the movable tube moves down to its bottom position, the suspended iron dust is ignited by an electric spark. A flame starts to propagate through the metal particle cloud. Using this chamber, the flame can propagate in an open field without any influence of the chamber wall in inducing the turbulence generation.

Moreover, Sun et al. [5,7,8] and Han et al. [9] precisely stated that the flame propagates at the constant velocity through particles cloud and the steady-state condition is an acceptable assumption for this simulation. In addition, Goroshin et al. [28] in the experimental study on the aluminum dust combustion enforced that the dust flame propagation in the tube can be divided into three different stages: laminar flame, oscillating flame, and turbulent accelerating flame. It is interesting to note that for very rich mixtures ($\geq$500 g/m^3), they observed the longest stage of laminar flame propagation. Sometimes, oscillations did not appear at all and the flame propagated in laminar mode until the end of the tube. The same phenomenon has been also observed during lycopodium combustion conducted by Berlad et al. [29].

In addition, Goroshin et al. [30] explained that taking into account the experimental difficulty in observing the combustion of individual particles in a dense suspension, the use of a laminar flame stabilized in a flow of dusty gas provides a feasible alternative. Unlike the highly transient phenomena associated with particle clouds ignited by shock waves or in turbulent reacting flows, a stabilized laminar flame provides a steady-state process [30] in which the process of particle combustion is spatially separated, similar to a laminar flame in gases. Thus, measurement of the spatial variations through a stabilized laminar flame replaces the necessity of time resolved measurements of transient particles combustion. It is worth noticing that many researchers have considered the one-dimensional simulation of flame propagation through particles cloud [28,31–36] and the steady-state condition [11–13,28,32–34]. According to the aforementioned points, a one-dimensional and steady state model is considered in the present research.

The main purpose of analyzing the flame propagation through a dust cloud is to obtain the particle concentration distribution on the leading edge of the combustion zone (i.e., unburned zone). Indeed, this feature will influence the lower flammability limits of combustible particle clouds [7]. The particles concentration just ahead of the combustion zone could be high enough to sustain the flame propagation, even if the average particle concentration is not high. This could be one of the main reasons why the lower flammability limit (equivalence ratio) of dust cloud flame is much smaller than that of gas fuel flame [7]. It is needed to note that the gas expansion rate is not too much in the unburned zone. But, behind the leading edge of the combustion zone (i.e., in the reaction zone), the particle number density decreases quickly. This decrease might be caused by the expansion of gas with temperature rise and by the velocity change of the particles [7,8], while the dynamic behavior of particles in the reaction zone is not the objective of this analytical model. The principal aim of this research is to investigate the concentration and velocity profiles of particles in the unburned zone and as mentioned before, the necessity and importance of this zone in the flammability limit is emphasized by the researchers [7–9] in their experimental studies.

Since the boiling point of iron (3023 K) is much higher than the adiabatic temperature of iron particle cloud (2285 K), no flame is seen in the gas phase [5]. This implies that sufficient iron vapor for sustaining a flame in the gas phase is not ejected from the particle surface, even during its combustion.

The combustion mechanisms of solid iron burning in pure oxygen have been studied [37,38] and a model of the iron oxidation process was proposed. They indicated that the oxidation process consists of the following stages [5]:

I. The reaction at the oxygen–oxide interface including the following fundamental steps:
   1. Oxygen molecules are physically adsorbed on the oxide surface.
   2. Physically adsorbed oxygen molecules dissociate and the oxygen atoms are chemically adsorbed on particular sites on the oxide surface.
   3. The chemically adsorbed oxygen atoms are incorporated in the oxide.

II. The diffusion of oxygen ions through the oxide layer.

III. The reaction at the metal–oxide interface.

A schematic of this process is observed in Fig. 1(b). Among the aforementioned steps, step (I) is much slower than the other steps [5]. The average diameter of burned iron particles is larger than that of unburned ones. This increase in the diameter is definitely brought by the reaction process. The average diameter of burned iron particles is 1.2 times larger than that of unburned iron particles [5], and the mass of each particle increases due to the oxidation by combustion.

In the Lagrangian approach to particle transport, particle Brownian motion is neglected and individual particle trajectories (position and velocity as a function of time) are determined by integrating the following system of ordinary differential equations:

$$\frac{dx_p}{dt} = V_p, \quad m_p \frac{dV_p}{dt} = F_D + F_G + F_B + F_T \tag{1}$$

where x_p and m_p are the particle position and mass, respectively. In addition, V_p is the velocity of the particle. Also F_D, F_G, F_B and F_T are the fluid-drag, gravitation, buoyancy and thermophoretic forces, respectively.

3. Forces on particle

3.1. Drag force

A particle moving at a different velocity comparing with the velocity of the surrounding gas will experience a gas resistance or, in other words, a fluid-drag force. At low Reynolds numbers, the drag force on a rigid sphere of radius r_p is given by Stokesian approximation as:

$$F_D = 6\pi\mu r_p(V_f - V_p) \tag{2}$$

where μ and V_f are the gas viscosity and the flame velocity of micro-iron particles/air mixture, respectively. As seen in Eq. (2), the drag force is proportional to the particle size and the difference between the flame and particle velocities.

3.2. Gravitation and buoyancy forces

The gravitation and buoyancy forces acting on a spherical particle are given by:

$$F_G + F_B = -\frac{4}{3}\pi r_p^3(\rho_p - \rho_g)g \tag{3}$$

where ρ_p and ρ_g are the particle and gas densities, respectively, and g is the gravitational acceleration vector. The gas density is typically much smaller than the particle density in Eq. (3).

In the following discussion, two limiting cases characterizing the nature of the particle/gas interaction are described:

1. In the continuum limit, the gas surrounding the particle appears as a continuous fluid and traditional continuum fluid dynamics apply for fluid motion.
2. In the free-molecular limit, however, the discrete nature of the gas becomes important and individual molecule/particle collisions must be considered.

Discrimination between these two regimes is made by comparing the particle diameter to the gas mean free path (which is defined as the average distance a molecule travels between collisions with other gas molecules); a dimensionless parameter known as the Knudsen number is commonly used for these comparisons:

$$Kn = \frac{2\lambda}{d_p} \tag{4}$$

where d_p is the particle diameter and λ is the gas mean free path described as follows:

$$\lambda = \frac{\mu}{\phi \rho_g \bar{c}} \tag{5}$$

where $\bar{c}$ is the mean thermal velocity of the gas molecules which is calculated via following expression:

$$\bar{c} = \left(\frac{8RT}{\pi M}\right)^{1/2} \tag{6}$$

where R, T and M are the universal gas constant, gas temperature and molecular mass of gas, respectively. Also, ϕ, is a dimensionless parameter that depends on the kinetic-theory model used to define the gas mean free path: in this work the value $\phi = 0.491$ is considered [39].

A large Knudsen number ($Kn > 10$) corresponds to the free-molecular regime, while a small Knudsen number ($Kn < 0.1$) corresponds to the continuum regime.

3.3. Thermophoretic force

Particles suspended in a gas with a temperature gradient experience a force in the direction of decreasing temperature. The resulting motion of particles away from hot regions and towards cold regions is called thermophoresis. An accepted formulation for the thermophoretic force on a spherical particle was developed by Talbot et al. [40] in a review of thermophoresis:

$$F_T = -3\pi\mu d_p \nu K_T \frac{\nabla T}{T_u} \tag{7}$$

$$K_T = \frac{2C_s((k_g/k_p) + C_t Kn)}{(1 + 3C_m Kn)(1 + 2(k_g/k_p) + 2C_t Kn)} \tag{8}$$

where ∇T is the temperature gradient in the mixture of micro-iron particles and gas and T_u is the mean surrounding gas temperature around the particle which is equal to the unburned mixture temperature. In addition, ν, k_p, k_g, C_t, C_s and C_m are the gas kinematics viscosity, the gas and iron particle thermal conductivities, the thermal creep coefficient, temperature jump coefficient, and velocity jump coefficient, respectively. $C_t = 2.2$, $C_s = 1.147$ and $C_m = 1.146$ are recommended by Batchelor and Shen [18]. Talbot et al. [40] compared their correlation with other experiments data over a wide range of Knudsen numbers, and found that it agreed with available experimental data to within 20%.

In the continuum limit of small Kn the thermophoretic force approaches:

$$F_{T,continum} = -6\pi\mu^2 d_p \frac{C_s k_g}{k_p + 2k_g} \frac{\nabla T}{\rho_g T_u} \tag{9}$$

In the free molecule regime limit Eq. (7) approaches the limit first derived by Waldmann and Schmitt [41]:

$$F_{T,molecular} = -\frac{\pi}{2}\phi\mu\bar{c}d_p^2 \frac{\nabla T}{T_u} \tag{10}$$

Note that in the free-molecular limit the thermophoretic force is proportional to diameter squared and is independent of the gas pressure and the particle thermal conductivity. It is needed to mention that in the combustion of micro particles, the Kn is less than 0.1 (in the continuum limit) therefore the thermophoretic force corresponds to the continuum regime (Eq. (9)) is substituted into Eq. (1).

4. Analytical model

In order to obtain the temperature profile applicable in Eq. (9) for low Mach number flow, energy conservation equation in the gas phase of mixture under the assumption of steady state is written as follows:

$$\rho V_f C \frac{dT}{dx_p} = k_g \frac{d^2T}{dx_p{}^2} + Q\rho_g \dot{\omega}_{chem} \tag{11}$$

In relation to the energy equation, it should be noted that temperature–time history is converted to a temperature–position profile under the steady-state assumption. Indeed, this kind of formulation is used by lots of researchers for the analytical modeling of the flame structure through dust particles [11–13,28,33,34].

The following dimensionless parameters are introduced in the above equation.

$$\theta = \frac{T - T_u}{T_f - T_u} \tag{12}$$

$$\hat{x}_p = \frac{x_p}{D_{th}/V_f} = \frac{\rho_g V_f C}{k_g} x_p \tag{13}$$

where V_f, Q and $\dot{\omega}_{chem}$ are the flame velocity, the heat of reaction and the reaction rate. Also the heat capacity appearing in the above equation is a combination of the gas heat capacity (C_p) and that of the particles (C_s) which can be evaluated from the following expression:

$$C = C_p + \frac{4\pi r_p{}^3 C_s \rho_p \tilde{n}_s}{3\rho_g} \tag{14}$$

where $\tilde{n}_s$ is the average number density of particles.

In fact, in this research, the structure of flame propagation through iron dust particles is divided into three zones; an unburned zone, a reaction zone and a post flame zone, as seen in Fig. 1(a). The thickness of the combustion zone is found to be 4–5 mm [5] by measuring the distance from the leading edge of the combustion zone to the end line of clear luminous points on the high-speed photomicrographs. The temperature is about 900 K [6] at the leading edge of the combustion zone and then it goes up and down near the end of the combustion zone.

The main objective of this study is to analyze the dynamic behavior of particles in the unburned zone. The available particles in this zone are influenced by the reaction zone. The published experimental data [7–9] declare that the particles in the unburned zone represent two different dynamic behaviors due to the impressibility from the reaction zone. First, the particles near the flame front vary in velocity and concentration distribution in the direction to the front and then by distancing from the flame front, the velocity and concentration profiles remain constant and do not change toward the reaction zone. To obtain a solution mathematically, it is helpful to divide the preheating zone in the primary and secondary parts. Hence, these two dynamic behaviors of particles in the unburned zone can be better investigated by neglecting the

influence of the thermophoretic force at a distance far from the leading edge of the combustion zone.

Eliminating the reaction term in unburned zone and applying the appropriate boundary conditions culminate in the following expression for temperature profile:

$$\theta = \exp(-\hat{x}_p) = \exp\left(-\frac{\rho_g V_f C}{k_g} x_p\right) \tag{15}$$

The above equation represents that at a distance far from the flame front, $x = +\infty$, $T = T_u$ and at the adjacent of leading edge of the reaction zone, $x = 0$, $T = T_f$. At the interface of the primary and secondary preheating zones:

$$\text{at}: \quad \hat{x}_p = \hat{x}_s \Rightarrow \theta = \theta_s \tag{16}$$

where $\theta_s = (T_s - T_u)/(T_f - T_u)$. Also, T_s is the temperature at the interface of the primary and secondary preheating zones. Inserting (16) into the dimensionless temperature Eq. (15) yields:

$$x_s = -\frac{k_g}{\rho_g V_f C} \ln \theta_s \tag{17}$$

Substituting Eqs. (2), (3) and (9) into Eq. (1) leads to:

$$m_p \frac{dV_p}{dt} = 6\pi\mu r_p (V_f - V_p) - \frac{4}{3}\pi r_p^3 (\rho_p - \rho_g) g - 12\pi\mu^2 r_p \frac{C_s k_g}{k_p + 2k_g} \frac{\nabla T}{\rho_g T_u} \tag{18}$$

Inserting T, ∇T from Eqs. (12) and (15), respectively, in the above correlation yields:

$$m_p \frac{dV_p}{dt} = 6\pi\mu r_p (V_f - V_p) - \frac{4}{3}\pi r_p^3 (\rho_p - \rho_g) g + 12\pi\mu^2 r_p \frac{C_s k_g}{k_p + 2k_g} \frac{\rho_g V_f C}{k_g} \frac{(T_f - T_u)}{\rho_g T_u} \exp\left(-\frac{\rho_g V_f C}{k_g} x_p\right) \tag{19}$$

In order to analytically solve the above equation, two principal assumptions are made in this research:

1. The term dV_p/dt is replaced by $V_p dV_p/dx$ in order to determine the variation of velocity and concentration as a function of the distance from the leading edge of the combustion zone. Indeed, according to a series of high-speed video images, Sun et al. [7,8] indicated that the combustion zone propagates upward at an almost constant velocity through two-phase mixture of iron particles and air. It was seen that at the ignition stage the flame shape is irregular and unsteady (in case the spark influences the flame propagation). At about 40 ms after ignition (i.e., about 15 mm from the ignition point) the flame begins to propagate spherically and its propagating velocity is almost constant with the time during the measurement [5]. Therefore, the steady-state condition can be considered at 15 mm from the ignition point (i.e., 40 ms after the ignition time) and thus, the velocity and concentration profiles achieved at 40 ms are validated for anytime. It is worth noting that according to the published experimental data [7,8], since the velocity and concentration profiles of particles across the flame propagation through iron dust cloud have been illustrated based on one-dimensional function of distance from the leading edge of the combustion zone and the vital aspects in the dynamic behavior of particles are to determine these profiles in the unburned zone, velocity–time history (i.e., Lagrangian method) of particles across flame propagation through iron dust cloud is converted to a velocity–position profile (i.e., Eulerian formulation).
2. Moreover, the drag force is neglected in comparison with gravitation, buoyancy and thermophoretic forces, so that the explicit description for the particle velocity is extracted. In fact, introducing the drag force into Eq. (19) leads to a nonlinear equation which cannot be solved by the analytical methods. It is noticeable that the main intention of this research is to propose a theoretical insight into the fundamental aspects of dynamic behavior of particles across flame propagation through a two-phase medium consisting of micro-iron particles and air. In addition, as known, the drag force should be applied into the governing equation due to the velocity difference between the gas and the particle. Since the iron dust particles just ahead of the reaction zone move in the same direction of the bulk gaseous motion in the unburned zone, the velocity difference between the gas and the particle in this situation is lower than that, at a distance far from the flame front. Therefore, the drag force is neglected in the governing equation and its effect is introduced into the boundary condition of particle velocity defined in a distance far from the leading edge of the combustion zone.

These assumptions are applied into Eq. (19) and after solving this equation, the following expression is extracted:

$$m_p \frac{V_p^2}{2} = -\frac{4}{3}\pi r_p^3 (\rho_p - \rho_g) g x_p - 12\pi\mu^2 r_p \frac{C_s k_g}{k_p + 2k_g} \frac{T_f - T_u}{\rho_g T_u} \times \exp\left(-\frac{\rho_g V_f C}{k_g} x_p\right) + const \tag{20}$$

In order to calculate the constant coefficients, it is necessarily needed to point out that the role of thermophoretic force is negligible at the specific distance from the flame front (L_t) and therefore, the particles fall gravitationally at the constant velocity U_t. So, at this specific length the balance between drag, buoyancy and gravitation forces culminates to a correlation for U_t as follows:

$$U_t = \frac{2}{9} \frac{g r_p^2}{\mu} (\rho_p - \rho_g) \tag{21}$$

Thus, the boundary condition is defined as:

$$\text{at}: \quad x = L_t \rightarrow V_p = -U_t \tag{22}$$

where L_t is described by the following equation which indicates a remarkable compatibility with the experimental results:

$$L_t = \left(\frac{\tilde{N}_s}{\rho_p}\right)^{-0.3} \left(\frac{\rho_g V_f C}{k_g} D\right)^{0.4} \left(\frac{\rho_g (U_t + V_f) d_p}{\mu}\right)^{3.2} x_s$$

$$\text{at}: \begin{cases} 15 \le V_f \le 35 (\text{cm/s}) \\ 0.1 \le \theta_s \le 0.4 \end{cases} \tag{23}$$

where $\tilde{N}_s$ and D are the particle dust concentration in a distance far from the leading edge of the combustion zone and the diameter of combustion chamber, respectively.

The boundary condition (22) is used for determining the particle velocity as a function of distance from the leading edge of the combustion zone as:

$$\frac{m_p}{2}(V_p^2 - U_t^2) = -\frac{4}{3}\pi r_p^3 (\rho_p - \rho_g) g (x_p - L_t) - \frac{12\pi\mu^2 r_p C_s (T_f - T_u) k_g}{(k_p + 2k_g)\rho_g T_u} \times \exp\left(-\frac{\rho_g V_f C}{k_g} L_t\right) \left(\exp\left\langle -\frac{\rho_g V_f C}{k_g} (x_p - L_t) \right\rangle - 1\right) \tag{24}$$

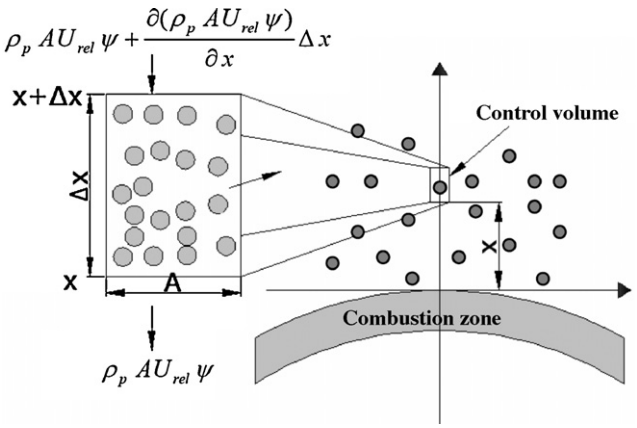

Fig. 2. Control volume on the leading edge of the combustion zone for determining the number density of iron particles.

Since the particle velocity is obtained as a function of the distance from the leading edge of the combustion zone, the variation of particle concentration can be represented. For the condensed phase (i.e., particles), the fractional volume is defined as:

$$\psi = \frac{n_s m_p}{\rho_p}, \quad \text{at}: \ x = L_t \rightarrow \psi = \tilde{\psi} \tag{25}$$

where n_s, m_p, ρ_p are the number density, mass of each particle and the density of particles, respectively. The control volume shown in Fig. 2 is used to estimate the number density of particles as a function of the distance from the leading edge of the combustion zone. The particle mass flux through a cross-sectional area of the control volume is $\rho_p AU_{rel}\psi$. Since the height of the control volume is Δx, the change in the flux is:

$$\frac{\partial \rho_p AU_{rel}\psi}{\partial x}\Delta x = \frac{\partial \rho_p U_{rel}\psi}{\partial x}A\Delta x \tag{26}$$

where U_{rel} (i.e., $V_p - V_f$), is the velocity of particles relative to leading edge of the combustion zone. The rate of particle mass accumulation in the control volume is $(\partial(\rho_p\psi)/\partial t)A\Delta x$. Since the iron particles are used in this study, the mass reduction rate due to vaporization is zero; while this rate cannot be neglected in the dust cloud including the volatile particles. Consequently, the mass conservation in the whole control volume is given by:

$$\frac{\partial(\rho_p\psi)}{\partial t}A\Delta x = \frac{\partial \rho_p U_{rel}\psi}{\partial x}A\Delta x \tag{27}$$

The flow condition in the region ahead of the combustion zone leading edge, can be considered to be steady state. The ratio of volume fraction and ratio of number density for micro-iron particles are gained by applying the boundary condition (25) into (27) as follows:

$$\frac{\psi}{\tilde{\psi}} = \frac{n_s}{\tilde{n}_s} = \frac{\tilde{U}_{rel}}{U_{rel}} \tag{28}$$

where

$$\tilde{\psi} = \frac{\tilde{n}_s m_p}{\rho_p}, \tilde{U}_{rel} = V_p\big|_{x_p = L_t} - V_f \tag{29}$$

5. Results and discussion

It should be noted that the agglomeration of particles in experimental simulations of dust combustion has been considered in this theoretical study. The diameters of most iron particles before the experiment are distributed from 1 to 5 μm based on the data supplied by manufacturing company, and also measured using a scanning electron microscope [7]. However, because small iron particles have very large specific surface energy, it is difficult to produce suspension of single particles. Most of particles would be agglomerated. According to one of the scanning electron microscope photographs of the iron particles sampled from the cloud in the combustion chamber at the ignition moment, Sun et al. [7] explained that most of the iron particles suspended in air have been agglomerated and most of the diameters of iron agglomerates are larger than 10 μm. It should be noted that the increase of iron particles diameter owing to the agglomeration has been considered in the present study (i.e., actual value of particle diameter is introduced in the calculated relations for the particle velocity profile and the particles concentration distribution). Interestingly, the agglomeration of dust particles is not only observed in the iron dust particles, but also in aluminum particles during dust combustion leading to incomplete combustion of aluminum and slag formation inside the combustion chamber. It is demonstrated that [42] coating aluminum with nickel reduced particle agglomeration during dust combustion.

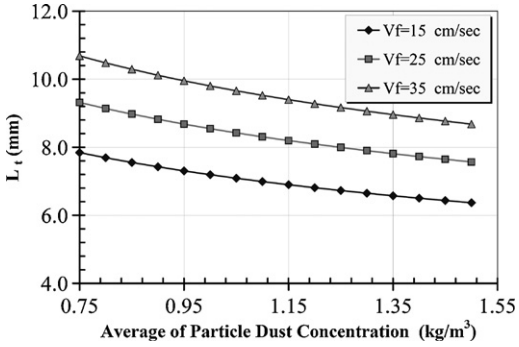

Fig. 3. The variation of L_t with the average of particle dust concentration for different flame propagation velocities through the mixture of micro-iron dust particles and air.

Fig. 3 shows the variation of L_t as a function of the average of dust particle concentration for different quantities of propagation velocity of flame through the mixture of micro-iron dust particles and air. As mentioned above, L_t is a length in which that the role of thermophoretic force is negligible and therefore, the particles fall gravitationally at the constant velocity U_t. According to Fig. 3, increasing the average of dust particle concentration at constant flame propagation velocity results in a decrease of L_t.

Fig. 4 illustrates the variation of L_t as a function of flame propagation velocity for different averages of dust particle concentration. As perceived, increasing the flame propagation velocity at constant number density of particles concludes in an approximately

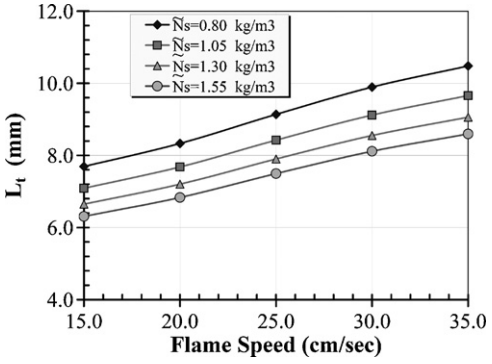

Fig. 4. The variation of L_t with the flame speed for different averages of particle dust concentration through the mixture of micro-iron dust particles and air.

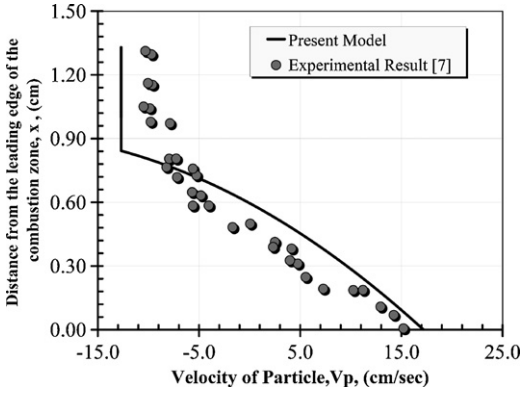

Fig. 5. The variation of particle velocity profile across the leading edge of the combustion zone at $\tilde{N}_s = 1.05\,\text{kg/m}^3$ and $V_f = 25\,\text{cm/s}$.

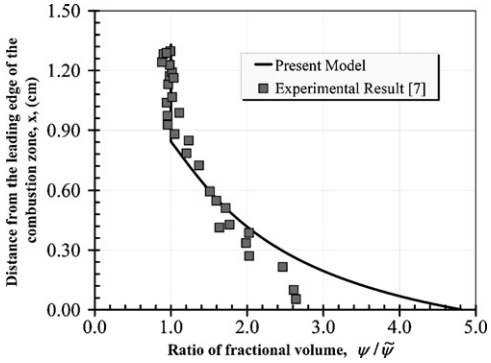

Fig. 7. The variation of the fractional volume ratio as a function of distance from the leading edge of the combustion zone at $\tilde{N}_s = 1.05\,\text{kg/m}^3$ and $V_f = 25\,\text{cm/s}$.

linear increase in L_t. It is worth noting that in the experimental study carried out for determining the density and velocity profiles by Sun et al. [7], the quantity of L_t was reported 10 mm at the constant $V_f = 25\,\text{cm/s}$ and $\tilde{N}_s = 1.05\,\text{kg/m}^3$ while the obtained data for L_t (Figs. 3 and 4) depicted from Eq. (23) at these conditions is equal to 8.6 mm which shows the reasonable compatibility with the aforementioned experimental data [7].

The velocity profile at $V_f = 25\,\text{cm/s}$ and $\tilde{N}_s = 1.05\,\text{kg/m}^3$ is depicted in Fig. 5 and compared with the experimental data [7]. As observed in this figure, increasing the distance from the leading edge of the combustion zone, firstly, the velocity profile varies from 17.16 cm/s on the flame front to −12.69 cm/s behind the leading edge of the combustion zone at the distance of $L_t = 8.6$ mm, after which it remains at the constant magnitude of −12.69 cm/s. The particle velocity profile has a good agreement with the published experimental result [7].

The relative velocity distribution across the leading edge of the combustion zone at $V_f = 25\,\text{cm/s}$ and $\tilde{N}_s = 1.05\,\text{kg/m}^3$ is illustrated in Fig. 6 and it is stated that the relative velocity distribution is 7.8 cm/s on the leading edge of the flame front and then it augments to 37.69 cm/s at $L_t = 8.6$ mm and after this distance from the leading edge of the combustion zone, the relative velocity distribution is remained constant at this value. It is needed to mention that the reported result from the presented analytical model is in a remarkable consistency with the published experimental data [7].

The ratio of fractional volume across the leading edge of the combustion zone at $V_f = 25\,\text{cm/s}$ and $\tilde{N}_s = 1.05\,\text{kg/m}^3$ is observed in Fig. 7. As depicted in Fig. 6, the relative velocity of the unburned iron particles decreases from L_t towards the leading edge of the combustion zone and it gains the minimum value on the flame

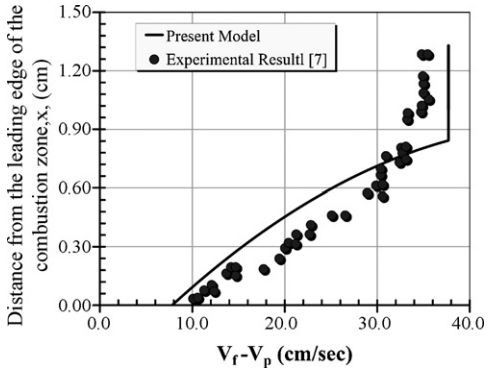

Fig. 6. The variation of relative velocity profile across the leading edge of the combustion zone at $\tilde{N}_s = 1.05\,\text{kg/m}^3$ and $V_f = 25\,\text{cm/s}$.

front. Therefore, according to Eq. (28), the particle agglomeration on the leading edge of the flame is more than the particle aggregation in a distance far from the flame front. Thus, it can be elucidated that the variation of the particle concentration has a considerable effect on the combustion reaction and flammability limit [7,8]. The obtained result has a partial agreement with the experimental data [7] implies that although this agreement is remarkable in the distance far from the leading edge of the combustion zone near by the leading edge of the flame front, it is not noticeable just ahead of leading edge of the combustion zone. A reason for this discrepancy is that just ahead of the combustion zone the assumption of one-dimensionality may not hold.

6. Conclusions

Since the flame structure depends on the behavior of dust particles, it is necessary to explore the movement of particles near the flame for the elucidation of dust flame propagation mechanism. Therefore, in this research the velocity and number density profiles of the micro-iron dust particles are analytically investigated. This study is based on utilizing the Lagrangian equation of motion and the effective forces such as thermophoretic, gravitation and buoyancy acting on the particles, in order to represent an analytical expression for the velocity profile. As observed in this investigation, the particle velocity reaches to its maximum value on the flame front and then it decreases to its minimum value at the distance of L_t, after which the particles fall gravitationally at the constant velocity U_t (due to the negligible effect of thermophoresis in this zone).

In the resumption, a control volume above the leading edge of the combustion zone is used for estimating the number density profile of micro-iron particles. This study clarifies that the particle dust concentration profile of micro-iron particles across the leading edge of the combustion zone changes at a distance shorter than L_t and it increases with the decrease in the distance from L_t to the leading edge of the combustion zone. This result indicates that, the particle concentration just ahead of the leading edge of the combustion zone becomes larger than that at a position far from the flame front. The increase in the number density of particles just ahead of the flame is an important phenomenon in the flame propagation through a particle cloud which definitely affects the lower flammability limits of the combustible mixture of particles cloud. The latter result of the aforementioned phenomenon is very important in prevention of dust explosion hazard. It is worth noticing that this analytical model is suitable for further improvement of numerical computer codes [43] (e.g., Dust Explosion Simulation Code (DESC)) to simulate the flame propagation in accidental dust explosions involving fine iron dust.

References

[1] R.K. Eckhoff, Dust Explosion in the Process Industries, second ed., Butterworth Heinemann, Oxford, 1997.
[2] K.L. Cashdollar, Overview of dust explosibility characteristics, J. Loss Prev. Process Ind. 13 (2000) 183–199.
[3] P.R. Amyotte, A. Basu, F.I. Khanb, Dust explosion hazard of pulverized fuel carryover, J. Hazard. Mater. 122 (2005) 23–30.
[4] G. Joseph, CSB hazard investigation team, combustible dusts: a serious industrial hazard, J. Hazard. Mater. 142 (2007) 589–591.
[5] J.H. Sun, R. Dobashi, T. Hirano, Combustion behavior of iron particles suspended in air, Combust. Sci. Technol. 150 (2000) 99–114.
[6] J.H. Sun, R. Dobashi, T. Hirano, Temperature profile across the combustion zone propagating through an iron particle cloud, J. Loss Prev. Process Ind. 14 (2001) 463–467.
[7] J.H. Sun, R. Dobashi, T. Hirano, Concentration profile of particles across a flame propagating through an iron particle cloud, Combust. Flame 134 (2003) 381–387.
[8] J.H. Sun, R. Dobashi, T. Hirano, Velocity and number density profiles of particles across upward and downward flame propagating through iron particle clouds, J. Loss Prev. Process Ind. 19 (2006) 135–141.
[9] O.S. Han, M. Yashima, T. Matsuda, H. Matsui, A. Miyake, T. Ogawa, A study of flame propagation mechanisms in lycopodium dust clouds based on dust particles' behavior, J. Loss Prev. Process Ind. 14 (2001) 153–160.
[10] K.L. Cashdollar, I.A. Zlochower, Explosion temperatures and pressures of metals and other elemental dust clouds, J. Loss Prev. Process Ind. 20 (2007) 337–348.
[11] M. Bidabadi, A. Rahbari, Modeling combustion of lycopodium particles by considering the temperature difference between the gas and the particles, Combust. Explos. Shock Waves 45 (2009) 49–57.
[12] M. Bidabadi, A. Rahbari, Novel analytical model for predicting the combustion characteristics of premixed flame propagation in lycopodium dust particles, J. Mech. Sci. Technol. 23 (2009) 2417–2423.
[13] M. Bidabadi, A. Haghiri, A. Rahbari, The effect of Lewis and Damköhler numbers on the flame propagation through micro-organic dust particles, Int. J. Therm. Sci. 49 (2010) 534–542.
[14] A. Gomez, D.E. Rosner, Thermophoretic effects on particles in counterflow laminar diffusion flames, Combust. Sci. Technol. 89 (1993) 335–362.
[15] N. Montassier, D. Boulaud, A. Renoux, Experimental study of thermophoretic particle deposition in laminar tube flow, J. Aerosol Sci. 22 (1991) 677–687.
[16] D.E. Rosner, D.W. Mackowski, P. Garcia-Ybarra, Size and structure insensitivity of the thermophoretic of aggregated soot particles in gases, Combust. Sci. Technol. 80 (1991) 87–101.
[17] O. Fujita, K. Ito, Observation of soot agglomeration process with aid of thermophoretic force in a microgravity jet diffusion flame, Exp. Therm. Fluid Sci. 26 (2002) 305–311.
[18] G.K. Batchelor, C. Shen, Thermophoretic deposition of particles in gas flowing over cold surfaces, J. Colloid Interface Sci. 107 (1985) 21–37.
[19] M.S. Joanne, W. Alan, H. Douglas, Soot and carbon deposition mechanisms in ethane/air flames, Fuel 74 (1995) 1753–1761.
[20] T. Pushkar, P.T. James, F. Xiaodong, R. Amy, Estimation of particle volume fraction, mass fraction and number density in thermophoretic deposition systems, Int. J. Heat Mass Transfer 46 (2003) 3201–3209.
[21] H. Ono, R. Dobashi, T. Sakuraya, Thermophoretic velocity measurement of soot particles under a microgravity condition, Proc. Combust. Inst. 29 (2002) 2375–2382.
[22] H. Ono, R. Dobashi, T. Sakuraya, Effect of thermophoresis on soot particles, in: Proceedings of the 39th Japanese Combustion Symposium, 2001, pp. 129–130 (in Japanese).
[23] R. Tsai, L.J. Liang, Correlation for thermophoretic deposition of aerosol particles onto cold plates, J. Aerosol Sci. 32 (2001) 473–487.
[24] F. Zheng, Thermophoresis of spherical and non-spherical particles: a review of theories and experiments, Adv. Colloid Interface Sci. 97 (2002) 255–278.
[25] C.C. Wang, Effect of thermophoresis on particle deposition rate from a natural convection flow onto a vertical wavy plate, Int. Commum. Heat Mass Transfer 32 (2005) 1337–1349.
[26] J.K. Walsh, A.W. Weimer, C.M. Hrenya, Thermophoretic deposition of aerosol particles in laminar tube flow with mixed convection, J. Aerosol Sci. 37 (2006) 715–734.
[27] Z. Chen, B. Fan, Flame propagation through aluminum particle cloud in a combustion tube, J. Loss Prev. Process Ind. 18 (2005) 13–19.
[28] S. Goroshin, M. Bidabadi, J.H.S. Lee, Quenching distance of laminar flame in aluminum dust clouds, Combust. Flame 105 (1996) 147–160.
[29] A. Berlad, H. Ross, L. Facca, V. Tangirala, Particle cloud flames in acoustic fields, Combust. Flame 82 (1990) 448–450.
[30] S. Goroshin, J. Mamen, A. Higgins, T. Bazyn, N. Glumac, H. Krier, Emission spectroscopy of flame fronts in aluminum suspensions, Proc. Combust. Inst. 31 (2007) 2011–2019.
[31] L.F. Ernst, F.L. Dryer, R.A. Yetter, T.P. Parr, D.M. Hanson-Parr, Aluminum droplet combustion in fluorine and mixed oxygen/fluorine containing environments, Proc. Combust. Inst. 28 (2000) 871–878.
[32] Y.L. Shoshin, E.L. Dreizin, Particle combustion rates for mechanically alloyed Al–Ti and aluminum powders burning in air, Combust. Flame 145 (2006) 714–722.
[33] Y. Huang, G.A. Risha, V. Yang, R.A. Yetter, Effect of particle size on combustion of aluminum particle dust in air, Combust. Flame 156 (2009) 5–13.
[34] K. Seshadri, A.L. Berlad, V. Tangirala, The structure of premixed particle–cloud flames, Combust. Flame 89 (1992) 333–342.
[35] D.P. Clark, L.D. Smoot, Model of accelerating coal dust flames, Combust. Flame 62 (1985) 255–269.
[36] J.H. Pickles, A model for coal dust duct explosions, Combust. Flame 44 (1982) 153–168.
[37] T. Hirano, J. Sato, Fire spread along structural metal pieces in oxygen, J. Loss Prev. Process Ind. 6 (1993) 151–157.
[38] J. Sato, K. Sato, T. Hirano, Fire spread mechanisms along steel cylinders in high pressure oxygen, Combust. Flame 51 (1983) 279–287.
[39] M.D. Allen, O.G. Raabe, Re-evaluation of Millikan's oil drop data for the motion of small particles in air, J. Aerosol Sci. 6 (1982) 537–547.
[40] L. Talbot, R.K. Cheng, R.W. Schefer, D.R. Willis, Thermophoresis of particles in a heated boundary layer, J. Fluid Mech. 101 (1980) 737–758.
[41] L. Waldmann, K.H. Schmitt, in: C.N. Davies (Ed.), Thermophoresis and Diffusiophoresis of Aerosols, Aerosol Science, Academic Press, New York, 1966.
[42] T.A. Andrzejak, E. Shafirovich, A. Varma, Ignition mechanism of nickel-coated aluminum particles, Combust. Flame 150 (2007) 60–70.
[43] T. Skjold, Review of the DESC project, J. Loss Prev. Process Ind. 20 (2007) 291–302.